

Magic high-order harmonics from a quasi-one-dimensional hexagonal solid

G. P. Zhang*

Department of Physics, Indiana State University, Terre Haute, Indiana 47809, USA

Y. H. Bai

Office of Information Technology, Indiana State University, Terre Haute, Indiana 47809, USA

(Received 3 February 2019; revised manuscript received 14 March 2019; published 28 March 2019)

High-order harmonic generation (HHG) from atoms is a coherent light source that opens up attosecond physics, but it is the application of HHG to solids that has brought much excitement in the last decade. Here we report a special kind of harmonics in a quasi-one-dimensional and hexagonal barium titanium sulfide: Under circularly polarized laser excitation, harmonics are generated only at first, fifth, seventh, and eleventh orders. These magic harmonics appear only with circularly polarized light, not with linearly polarized light. Neither cubic nor tetragonal cells have magic harmonics even with circularly polarized light. Through a careful group-theory analysis, we find that two subgroups of symmetry operations unique to the hexagonal symmetry cancel out third and ninth harmonics. This feature presents a rare opportunity to develop HHG into a crystal-structure characterization tool for phase transitions between hexagonal and nonhexagonal structures.

DOI: [10.1103/PhysRevB.99.094313](https://doi.org/10.1103/PhysRevB.99.094313)**I. INTRODUCTION**

High-order harmonic generation (HHG) from solids [1] and nanostructures [2–5] has been extended to a broad scope of materials (see references in [6–8]). With strong signals and large tunability of energy spectra, solid-state HHG has reshaped the landscape of HHG as a radiation source from simple atoms, and has gradually developed into a practical tool to characterize materials properties on unprecedented short-time scales, where the motion of electrons can be pictured frame by frame within several hundred attoseconds. Naturally, not all the processes such as chemical reactions require such short-time scales, but many do. For instance, to resolve laser-induced ultrafast spin dynamics [9], a short pulse is necessary, since it allows one to disentangle the magnetic and electronic dynamics from nuclear vibrational dynamics. However, condensed matters are far more complex than atoms. The advantage of HHG over other tools has not been materialized, though using HHG to map bands has been proposed [10].

Recently, BaTiS₃ shows a broadband birefringence in infrared regions [11], but it is its quasi-one-dimensionality and strong optical anisotropy that caught our attention. Low-dimensional materials with large oscillator strength are indispensable to nonlinear optical responses, if their band gaps (E_g) are small but nonzero. According to the well-known scaling rule, the third-order susceptibility $\chi^{(3)}$ is proportional to $\chi^{(3)} \propto E_g^{-6}$ [12,13]. BaTiS₃ has a tiny gap, so even within a perturbation limit, its nonlinear susceptibility is expected to be strong, but little is known about its nonlinear optical properties, and even less its high-order harmonic generation.

In this paper, we predict strange high-order harmonics in hexagonal barium titanium sulfide (BaTiS₃) that circularly

(σ) polarized light generates harmonics only at a few special orders. Regardless of laser pulse duration and photon energy, σ light only induces first, fifth, seventh, and eleventh harmonics, not third and ninth harmonics. We call them magic harmonics. Linearly (π) polarized light only generates normal odd-order harmonics. This finding is independent of whether or not the system has an inversion symmetry. Neither cubic nor tetragonal systems have magic harmonic orders even excited with σ light. We carry out a detailed group symmetry analysis and find that magic harmonics are associated with the hexagonal group symmetry [14–17]. This group contains two subgroups: subgroup A contains the identity matrix and 180° rotation, and subgroup B includes the four proper rotations, C_6 , C_6^2 , C_6^4 , and C_6^5 . Each subgroup only generates a normal harmonic spectrum, but if they both are present, they generate a destructive interference and exactly cancel out harmonics at the third and ninth orders. The same conclusion is found for the six improper rotations. Since cubic or tetragonal systems do not have such magic harmonics, magic harmonics found here present an opportunity to develop HHG into a possible structure characterization tool for phase transitions between hexagonal and nonhexagonal structures [18] in varieties of materials [19–28]. Our finding complements the prior studies using linearly polarized light [6,29,30] well.

The rest of the paper is arranged as follows. In Sec. II, we outline our theoretical formalism. Our main results are presented in Sec. III, where we provide the details of our structural optimization, information of the electronic states, and high harmonic generations, followed by a symmetry group analysis. Finally, we conclude this paper in Sec. IV.

II. THEORETICAL FORMALISM

BaTiS₃ is a quasi-one-dimensional material with Ti and S atoms forming a chain along the c axis, with chain-chain

*guo-ping.zhang@outlook.com

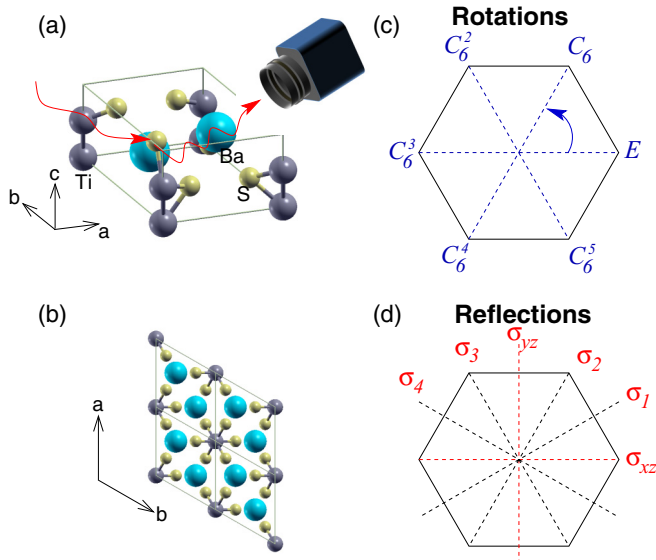


FIG. 1. High harmonic generation in BaTiS_3 . (a) Unit cell of BaTiS_3 with group symmetry $P6_3mc$ has no inversion symmetry. The laser polarization can be either in the xy (ab) plane or along the z (c) axis. Harmonics can be detected by a camera. (b) The same structure projected in the ab plane, with two units along the a and b axes. (c) Six symmetry rotations in the ab plane can be separated into two subgroups, A ($E, C_6, C_6^2, C_6^3, C_6^4, C_6^5$) and B (C_6, C_6^2, C_6^4, C_6^5). These two subgroups are the cause of magic harmonics. (d) Six improper rotations can also be categorized into two subgroups, A (σ_{yz}, σ_{xz}) and B ($\sigma_1, \dots, \sigma_4$).

distance of 6.749 Å. Figure 1(a) shows its crystal structure. Ti chains pass through face-sharing sulfur octahedra. Figure 1(b) shows its structure projected onto the ab plane, where S atoms form a distinctive hexagonal motif and Ba atoms fill the empty space left behind. According to Huster [31] and Singh *et al.* [11], BaTiS_3 adopts a hexagonal BaNiO_3 structure with space group no. 194, $P6_3/mmc$. This structure has an inversion symmetry, with Ti at the Wyckoff position ($2a$), Ba at ($2d$), and S at ($6h$). Table I shows the Huster's structure information. However, Niu *et al.* [11] suggested a different space group no. 186, $P6_3mc$, which has a lower symmetry without inversion symmetry and the number of symmetry operations is reduced from 24 to 12. Which structure, Niu's or Huster's, is more stable is an open question.

Theoretically, we employ the state-of-the-art density functional theory [32] to optimize the BaTiS_3 structure, with little input from the experiments. We first solve the Kohn-Sham

TABLE I. Wyckoff positions of BaTiS_3 determined by Huster [31]. His structure is of BaNiO_3 -type and has symmetry group no. 194, $P6_3/mmc$. This structure has an inversion symmetry. The lattice constants are $a = 6.756(1)$ Å and $c = 5.798(1)$ Å.

Atom	Position	x	y	z
Ti	$2a$	0	0	0
Ba	$2d$	$\frac{1}{3}$	$\frac{2}{3}$	$\frac{3}{4}$
S	$6h$	0.1655(10)	0.3310(10)	$\frac{1}{4}$

equation [32–34],

$$\left[-\frac{\hbar^2 \nabla^2}{2m_e} + V_{ne} + V_{ee} + V_{xc} \right] \psi_{i\mathbf{k}}(\mathbf{r}) = E_{i\mathbf{k}} \psi_{i\mathbf{k}}(\mathbf{r}), \quad (1)$$

where m_e is the electron mass, the terms on the left-hand side represent the kinetic energy, nuclear-electron attraction, electron-electron Coulomb repulsion, and exchange correlation [35], respectively. $\psi_{i\mathbf{k}}(\mathbf{r})$ is the Bloch wave function of band i at crystal momentum \mathbf{k} , and $E_{i\mathbf{k}}$ is the band energy. We include the spin-orbit coupling (SOC) using a second-variational method in the same self-consistent iteration [32], though we find the effect of SOC is very small. WIEN2K [32] employs the linearized augmented plane-wave basis. In our calculation, the dimensionless product of plane-wave cutoff K_{\max} and muffin-tin radius R is $RK_{\max} = 9$. Such a large value ensures that even higher eigenstates are accurately described. The muffin-tin radius for each element is as follows: $R_{\text{mt}}(\text{Ba}) = 2.5$ bohr, $R_{\text{mt}}(\text{Ti}) = 2.32$ bohr, and $R_{\text{mt}}(\text{S}) = 2.06$ bohr, so the core charges are confined within the spheres. We use a \mathbf{k} mesh of $23 \times 23 \times 24$, which is more than enough to converge our results.

To simulate HHG, we employ a laser pulse with duration 48 fs and photon energy 1.6 eV. These laser parameters are commonly used in experiments. We numerically solve the time-dependent Liouville equation for density matrices $\rho_{\mathbf{k}}$ at each \mathbf{k} [33]

$$i\hbar \frac{\partial \rho_{\mathbf{k}}}{\partial t} = [H, \rho_{\mathbf{k}}], \quad (2)$$

where H contains both the system Hamiltonian and the interaction between the laser and system. The expectation value of the momentum operator [3,36] is computed from

$$\mathbf{P}(t) = \sum_{\mathbf{k}} \text{Tr}[\rho_{\mathbf{k}}(t) \hat{\mathbf{P}}_{\mathbf{k}}], \quad (3)$$

where the trace is over band indices and crystal momentum \mathbf{k} . We include all the states from band 41 to 146 [see the arrows in Fig. 2(a)], which cover a major portion of the energy spectrum. Calculations using different parts of the energy spectrum are also carried out, but there is no qualitative difference. To compute the harmonic signal, we Fourier transform $\mathbf{P}(t)$ to the frequency domain (see details in Ref. [7]),

$$\mathbf{P}(\Omega) = \int_{-\infty}^{\infty} \mathbf{P}(t) e^{i\Omega t} \mathcal{W}(t) dt, \quad (4)$$

where $\mathcal{W}(t)$ is the window function. Each component of $\mathbf{P}(\Omega)$ requires a separate Fourier transform. We find that the window function is necessary since small oscillations in $\mathbf{P}(t)$ at the end of the time window easily hide the harmonic structures at high orders. We emphasize that this window function does not alter the amplitude of the harmonic signal. We choose a hyper-Gaussian $\mathcal{W}(t) = \exp[-b(at)^8]$, where a and b determine the width of the window function and the starting and ending times. In our current study, we use $a = 0.035/\text{fs}$ and $b = 5 \times 10^{-9}$ (no unit), which spans the entire region of our data.

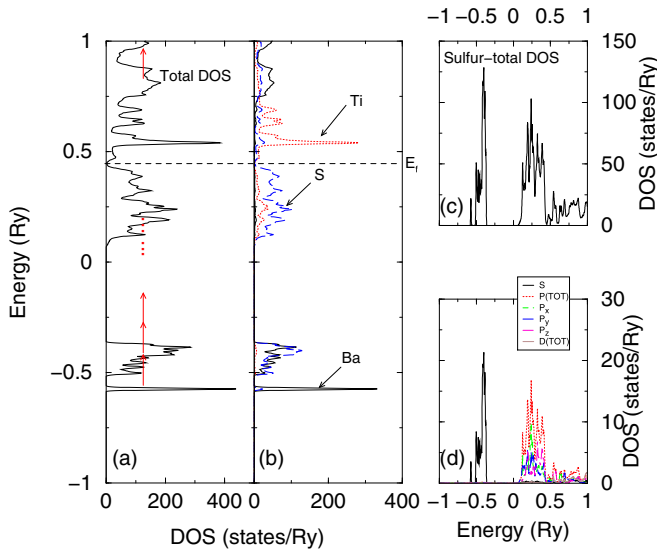


FIG. 2. (a) Total density of states (DOS). The arrows highlight the excitation process of our laser pulse. States from 41 to 146 are included in our calculation. The Fermi level is denoted by a horizontal dashed line. (b) Element-resolved partial DOS, where the states around the Fermi level are dominated by Ti and S atoms. (c) Partial density of states for sulfur, which is further decomposed into different orbital characters in (d).

III. RESULTS

A. Structural optimization

Since earlier studies by Huster [31], structurally Niu and co-workers [11] provided two possible structures for BaTiS₃ with the same group symmetry. According to the international tables for crystallography [37], in group 186 ($P6_3mc$), Ti Wyckoff positions are at $(2a)$ $(0, 0, z)$ and $(0, 0, z + 1/2)$, Ba positions are at $(2b)$ $(1/3, 2/3, z)$ and $(2/3, 1/3, z + 1/2)$, and S positions are at $(6c)$: $(x, -x, z)$, $(x, 2x, z)$, $(-2x, -x, z)$, $(-x, x, z + 1/2)$, $(-x, -2x, z + 1/2)$, and $(2x, x, z + 1/2)$. However, Niu's positions [11] are not compatible with these positions. For instance, Niu's second set of the S position is at $(0.8301, 0.6603, 0.850)$, but it should be $(0.8301, 0.1699, 0.350)$. Their y position can be reproduced by $2x - 1$, where x is the x position; also one has to subtract $1/2$ from their z position. In the following we first correct their Wyckoff positions and then carry out the calculation. Our Wyckoff positions are in compliance with the international tables for crystallography.

We optimize both their structures, and find that the first structure after optimization has a total energy lower than the second structure by 4 mRy. Both the structures have a lower energy than Singh's structure. Our theoretical results support a structure with group symmetry $P6_3mc$. This is the first testable case for future experiments. Our theoretically optimized Wyckoff positions, together with the corrected experimental positions from Niu's paper [11], are listed in Table II.

TABLE II. Optimized Wyckoff positions of BaTiS₃, with group no. 186, $P6_3mc$, and lattice constants $a = 6.749 \text{ \AA}$, $b = 6.749 \text{ \AA}$, and $c = 5.831 \text{ \AA}$. S atoms are at $6c$ positions $(x, -x, z)$, $(x, 2x, z)$, $(-2x, -x, z)$, $(-x, x, z + 1/2)$, $(-x, -2x, z + 1/2)$, and $(2x, x, z + 1/2)$. This structure has no inversion symmetry. The experimental results from Niu *et al.* [11] are shown in the parentheses. If there is no difference between their experiment and our theory, only one entry is listed.

Atom	Position	x	y	z
Ba	$2b$	$\frac{1}{3}$	$\frac{2}{3}$	0.2989 (0.298)
Ti	$2a$	0	0	0.5067 (0.522)
S	$6c$	0.8329 (0.8301)	0.1671 (0.1618)	0.2875 (0.298)

B. Electronic states

Before we present the high harmonic generation spectrum of BaTiS₃, we first investigate its electronic structures. Figure 2(a) shows our total density of states (DOS). The Fermi energy (E_f) is denoted by a dashed line. Consistent with Singh's results ($E_g = 0.01 \text{ eV}$) [11], our energy gap is very small, around $E_g = 0.014 \text{ eV}$, on the energy scale of room temperature. We expect some important thermal-electric applications. Figure 2(b) shows the element-resolved partial density of states. We notice that Ba has a large contribution only in the lower energy window about 1 Ry below the Fermi level. Ti (dotted line) and S (dashed line) atoms dominate DOS around the Fermi level. The partial DOS for S is shown in Fig. 2(c), which is further resolved into different orbitals in Fig. 2(d). It is clear that the states at -0.5 Ry are $3s$ states, while its $3p$ states are just around the Fermi level. As seen below, these states provide a channel for HHG.

C. High harmonic generation

We start with the structure with group symmetry $P6_3/mmc$ [11,31]. We align the laser polarization along the x axis. Figure 3(a) shows the harmonic spectrum on a logarithmic scale as a function of harmonic orders. We see that all the harmonics appear at odd orders along the x axis, which is the original laser polarization direction. The signals along the y and z axes are at the noise level and not shown. Next, we use Niu's experimental structure with group symmetry $P6_3mc$. Figure 3(b) shows that under the same laser condition, the harmonic signals along the x axis for these two structures are identical [compare Figs. 3(a) and 3(b)], where all the harmonics are at odd orders. However, qualitative differences are observed along the z axis. $P6_3mc$ has no inversion symmetry and harmonics along the z axis appear at even orders. This agrees with the symmetry properties with this group symmetry [15,17] that the even orders only appear when the laser polarization is along the z axis. Consistent with Niu's observation of strong optical anisotropy [11], our zeroth-order harmonic signal along the c axis is particularly strong; and to obtain clean harmonics at high orders, we subtract $\mathbf{P}(-\infty)$ from $\mathbf{P}(t)$ before we compute the power spectrum shown in Fig. 3(b). This is our second testable result: If Huster's structure is correct, no harmonic signal along the z direction is present; if Niu's structure is correct, even harmonics along the z axis appear.

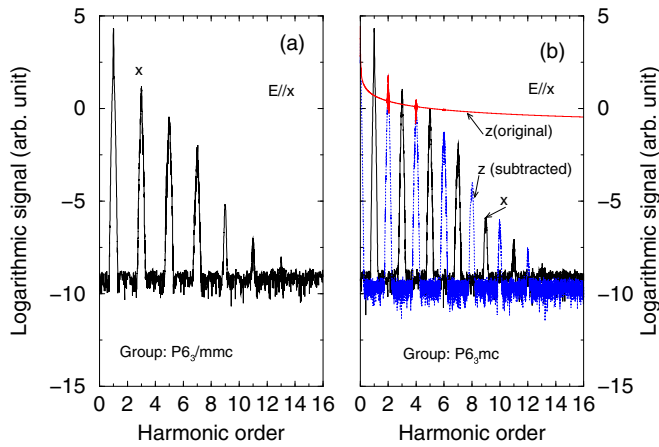


FIG. 3. (a) Logarithmic of high harmonic spectrum as a function of harmonic order under x -linearly polarized laser excitation. The crystal structure has group symmetry $P6_3/mmc$ and has inversion symmetry. All the harmonics along the x axis are odd orders. Signals along the other axes are at noise level. (b) Harmonic signals for the same laser pulse but for the structure with group symmetry $P6_3mc$. This structure has no inversion symmetry, so the even order harmonics appear along the c (z) axis (dashed line). The signal along the x axis is similar to (a). The z component of harmonics without treatment is shown on the top. Since the signal along the z axis is too strong, we subtract its initial value $\mathbf{P}(-\infty)$ from $\mathbf{P}(t)$ and then carry out the Fourier transformation to get a “cleaner” spectrum labeled with “ z (subtracted)”. Even harmonic only appears when the laser polarization is along the z axis [15,17].

The structural symmetry is not the only information that HHG can reveal. When we employ circularly polarized light (σ), to our surprise, some harmonics are mysteriously missing. Figure 4(a) shows that the third and ninth harmonics disappear. Only the first, fifth, seventh, and eleventh harmonics remain, magic harmonics. These magic harmonics do not depend on whether the group symmetry is $P6_3/mmc$ [Fig. 4(a)] or $P6_3mc$ [Fig. 4(b)]. Therefore, the common symmetry operations shared by these two space groups must be at the root of these magic harmonics. However, since we have a huge number of \mathbf{k} points, it is a challenge to determine the origin of these magic harmonics. We decide to select a single \mathbf{k} point and resolve $\mathbf{P}_{\mathbf{k}}(t)$ according to its 12 symmetry operations,

$$\mathbf{P}_{\mathbf{k}}(t) = \sum_{s=1}^6 \mathbf{P}_{\mathbf{k}}^s(t) + \sum_{q=1}^6 \mathbf{P}_{\mathbf{k}}^q(t), \quad (5)$$

where s refers to six proper rotations [see Fig. 1(c)] and q runs over six improper rotations (reflections) [Fig. 1(d)]. We symmetry-resolve $\mathbf{P}_{\mathbf{k}}(t)$, not its Fourier transformed $\mathbf{P}_{\mathbf{k}}(\omega)$, because the interference only occurs in the time domain, not in the frequency domain. Equation (5) is seemingly simple, but harbors too many possible combinations,

$$\sum_{i=1}^{12} \binom{i}{12}.$$

Lax [38] has an example of an equilateral triangle, with six symmetry operations. His example cannot directly apply to

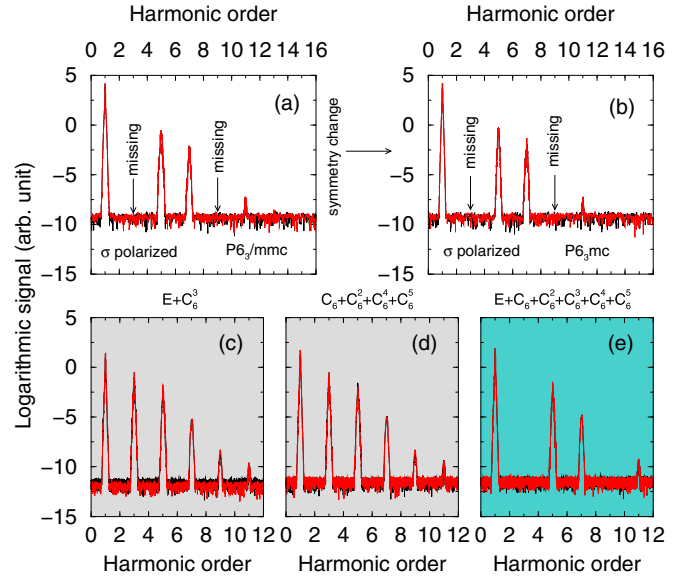


FIG. 4. (a) Magic high-order harmonics generated from BaTiS_3 with $P6_3/mmc$ symmetry under circularly polarized light (σ) in the xy plane, where third and ninth harmonics are missing. The light polarization plane is within the ab plane [see Fig. 1(b)]. Note that the x and y components are indistinguishable within numerical accuracy. (b) Magic harmonics are also present in BaTiS_3 with a symmetry group $P6_3mc$ without inversion symmetry. (c) High-order harmonics at a crystal momentum point close to $(0.05, 0.05, 0)$. The results are similar for other \mathbf{k} points. The summation is over symmetry operations in subgroup A (E and C_6^3). The harmonics are normal. (d) Same as (c), but the summation is over symmetry elements in subgroup B (C_6 , C_6^2 , C_6^4 , C_6^5). These symmetry rotations keep Ti atoms intact while transforming S atoms into their equivalent positions [see Figs. 1(b) and 1(c)]. The harmonics are also normal and appear only at odd orders. (e) Summation of all the proper rotations on HHG signal reproduces magic harmonics seen in (a) and (b). It is the destructive interference between these two subgroups that cancels the third and ninth harmonics.

our problem, but we notice that in his diagram the triangle has a mirror plane which could cancel all the even-order harmonics. This motivates us to lay out all the proper rotations within the ab plane [Fig. 1(c)], where we label each vertex with a symmetry operation. C_6^3 is a 180° rotation with respect to the c axis, much like an inversion operation in the Lax’s example. We immediately recognize that the identity matrix E and rotation C_6^3 , or subgroup A below, ensure that even harmonics do not appear. This is verified by our calculation [see Fig. 4(c)], but their harmonics are normal, and no magic orders are observed. Note that the disappearance of the even harmonics does not contradict the symmetry properties because the even harmonics allowed by the symmetry $P6_3mc$ appears only when the electric field is along the z axis [15,17]. In our case, our laser field polarization is in the xy plane. Experimentally, Ghimire *et al.* [6], who employed linear polarization in the ab plane, also found no even order harmonics for ZnO which happens to have the same group symmetry $P6_3mc$. Therefore, our results are fully consistent with the symmetry requirement and prior experiments [6].

What about the remaining four proper rotations or subgroup B? If we compare Figs. 1(b) and 1(c), we notice that these symmetry operations bring S atoms to their equivalent positions while keeping Ti atoms intact. These four rotation matrices are

$$\begin{aligned}
 C_6(60^\circ) &= \begin{pmatrix} \frac{1}{2} & \frac{\sqrt{3}}{2} & 0 \\ -\frac{\sqrt{3}}{2} & \frac{1}{2} & 0 \\ 0 & 0 & 1 \end{pmatrix}, \\
 C_6^2(120^\circ) &= \begin{pmatrix} -\frac{1}{2} & \frac{\sqrt{3}}{2} & 0 \\ -\frac{\sqrt{3}}{2} & -\frac{1}{2} & 0 \\ 0 & 0 & 1 \end{pmatrix}, \\
 C_6^4(240^\circ) &= \begin{pmatrix} -\frac{1}{2} & -\frac{\sqrt{3}}{2} & 0 \\ \frac{\sqrt{3}}{2} & -\frac{1}{2} & 0 \\ 0 & 0 & 1 \end{pmatrix}, \\
 C_6^5(300^\circ) &= \begin{pmatrix} \frac{1}{2} & -\frac{\sqrt{3}}{2} & 0 \\ \frac{\sqrt{3}}{2} & \frac{1}{2} & 0 \\ 0 & 0 & 1 \end{pmatrix}.
 \end{aligned} \tag{6}$$

We first check whether each pair of symmetry operations lead to magic harmonics, but this fails, so we simply combine all of them. The results are shown Fig. 4(d), where all the harmonics appear normal. Then we test whether mixing some improper rotations could cause magic harmonics, but it is unsuccessful. We also examine the prior results in magnetic monolayers with tetragonal symmetries [7], but we do not find any magic harmonics under the same laser condition. After long and difficult testing, we finally come to realize that the summation over all $\mathbf{P}_s(t)$ of the proper rotation might be able to reveal magic harmonics, and to our amazement, it indeed works. Figure 4(e) shows magic harmonics, with the third- and ninth-order harmonics missing. It is the destructive interference between two symmetry subgroups A and B that leads to magic harmonics. It is an easy task to extend this finding to improper rotations [see Fig. 1(d)]. Different from the proper rotations, the mirror image operations σ_{yz} and σ_{xz} form a subgroup, with the four remaining operations from σ_1 to σ_4 forming another subgroup. These two subgroups play the same role as the two subgroups for the proper rotations. Once we add their contributions up, we again reproduce the magic harmonics. We also examine other hexagonal systems and reach the same conclusion. These magic harmonics are

a hallmark of hexagonal structure, which is likely to have important applications in the future. For instance, hexagonal-cubic crystal structure transformation was found in many technologically important materials: aluminum nitride [19], GaN [20], BN [21–23], zinc oxynitride layers [24], NaYF₄ [25], Eu₂O₃ [26], CdTe [27], and others [28]. Our finding suggests a simple protocol to determine whether a hexagonal-cubic phase transition occurs by checking whether these magic harmonics appear.

IV. CONCLUSION

We have demonstrated magic high-order harmonics in hexagonal and quasi-one-dimensional solid BaTiS₃. Our results reflect the usefulness of group theory and the power of high harmonic generation as a structural characterization tool. Specifically, we show how harmonics are generated sensitively depends on crystal structures and laser polarization. Whether BaTiS₃ adopts $P6_3/mmc$ or $P6_3mc$ symmetry determines whether even order harmonics appear along the c axis. The qualitative difference is found under circularly (σ) polarized light excitation between the hexagonal structure for BaTiS₃ and tetragonal structure [7]. σ light produces no magic harmonics in tetragonal systems, but it generates magic harmonics in hexagonal systems. These magic harmonics are the hallmark of the hexagonal structure, and potentially provide a tool to investigate phase transitions in a wide scope of materials. One ideal system to realize our prediction could be BaVS₃. At room temperature BaVS₃ adopts $P6_3/mmc$ symmetry, but transforms to an orthorhombic structure between 70 and 240 K [39]. Therefore, our finding will motivate experimental and theoretical investigations in other research fields.

ACKNOWLEDGMENTS

We would like to thank Dr. D. Singh (University of Missouri) for sending us his structure file. This work was solely supported by the US Department of Energy under Contract No. DE-FG02-06ER46304. Part of the work was done on Indiana State University's high performance Quantum and Obsidian clusters. The research used resources of the National Energy Research Scientific Computing Center, which is supported by the Office of Science of the US Department of Energy under Contract No. DE-AC02-05CH11231.

-
- [1] Gy. Farkas, Cs. Tóth, S. D. Moustazis, N. A. Papadogiannis, and C. Fotakis, Observation of multiple-harmonic radiation induced from a gold surface by picosecond neodymium-doped yttrium aluminum garnet laser pulses, *Phys. Rev. A* **46**, R3605 (1992).
- [2] K. A. Pronin, A. Bandrauk, and A. A. Ovchinnikov, Harmonic generation by a one-dimensional conductor: Exact results, *Phys. Rev. B* **50**, 3473 (1994).
- [3] G. P. Zhang, Optical High Harmonic Generations in C₆₀, *Phys. Rev. Lett.* **95**, 047401 (2005).

- [4] R. Ganeev, L. Bom, J. Abdul-Hadi, M. Wong, J. Brichta, V. Bhardwaj, and T. Ozaki, Higher-Order Harmonic Generation from Fullerene by Means of the Plasma Harmonic Method, *Phys. Rev. Lett.* **102**, 013903 (2009).
- [5] R. A. Ganeev, *High-Order Harmonic Generation in Laser Plasma Plumes* (Imperial College Press, London, 2013).
- [6] S. Ghimire, E. Sistrunk, P. Agostini, L. F. DiMauro, and D. A. Reis, Observation of high-order harmonic generation in a bulk crystal, *Nat. Phys.* **7**, 138 (2011).

- [7] G. P. Zhang, M. S. Si, M. Murakami, Y. H. Bai, and T. F. George, Generating high-order optical and spin harmonics from ferromagnetic monolayers, *Nat. Commun.* **9**, 3031 (2018).
- [8] S. Y. Kruchinin, F. Krausz, and V. S. Yakovlev, Colloquium: Strong-field phenomena in periodic systems, *Rev. Mod. Phys.* **90**, 021002 (2018).
- [9] E. Beaurepaire, J. C. Merle, A. Daunois, and J.-Y. Bigot, Ultrafast Spin Dynamics in Ferromagnetic Nickel, *Phys. Rev. Lett.* **76**, 4250 (1996).
- [10] G. Vampa, T. J. Hammond, N. Thire, B. E. Schmidt, F. Legare, C. R. McDonald, T. Brabec, D. D. Klug, and P. B. Corkum, All-Optical Reconstruction of Crystal Band Structure, *Phys. Rev. Lett.* **115**, 193603 (2015).
- [11] S. Niu *et al.*, Giant optical anisotropy in a quasi-one-dimensional crystal, *Nat. Photon.* **12**, 392 (2018).
- [12] G. P. Agrawal, C. Cojan, and C. Flytzanis, Nonlinear optical properties of one-dimensional semiconductors and conjugated polymers, *Phys. Rev. B* **17**, 776 (1978).
- [13] G. P. Zhang, Frequency dependence of scaling exponents of hyperpolarizability in polyenes: A density-matrix renormalization-group approach, *Phys. Rev. B* **60**, 11482 (1999).
- [14] R. Hellwarth, Third-order optical susceptibilities of liquids and solids, *Prog. Quant. Electron.* **5**, 1 (1977).
- [15] P. N. Butcher and D. Cotter, *The Elements of Nonlinear Optics* (Cambridge University Press, Cambridge, UK, 1990).
- [16] C. Shang and H. Hsu, The spatial symmetric forms of third-order nonlinear susceptibility, *IEEE J. Quantum Electron.* **23**, 177 (1987).
- [17] R. W. Boyd, *Nonlinear Optics* (Academic, New York, 1991).
- [18] Y. A. Izyumov and V. N. Syromyatnikov, *Phase Transitions and Crystal Symmetry* (Kluwer, Dordrecht, 1990).
- [19] A. Iwata and J. Akedo, Hexagonal to cubic crystal structure transformation during aerosol deposition of aluminum nitride, *J. Cryst. Growth* **275**, e1269 (2005).
- [20] J. Menniger, U. Jahn, O. Brandt, H. Yang, and K. Ploog, Identification of optical transitions in cubic and hexagonal GaN by spatially resolved cathodoluminescence, *Phys. Rev. B* **53**, 1881 (1996).
- [21] H. J. Milledge, E. Nave, and F. H. Weller, Transformation of cubic boron nitride to a graphitic form of hexagonal boron nitride, *Nature (London)* **184**, 715 (1959).
- [22] J. Olander and K. Larsson, Initial growth of hexagonal and cubic boron nitride: A theoretical study, *Phys. Rev. B* **68**, 075411 (2003).
- [23] M. Halo, C. Pisani, L. Maschio, S. Casassa, M. Schütz, and D. Usvyat, Electron correlation decides the stability of cubic versus hexagonal boron nitride, *Phys. Rev. B* **83**, 035117 (2011).
- [24] M. Gomez-Castano, J. L. Puaa, and A. Redondo-Cubero, Identification of the cubic-to-hexagonal phase transition for the production of stable zinc oxynitride layers, *CrystEngComm* **20**, 3666 (2018).
- [25] S. Saha, R. G. S. Pala, and S. Sivakumar, Catalyzing cubic-to-hexagonal phase transition in NaYF₄ via ligand enhanced surface ordering, *Cryst. Growth Des.* **18**, 5080 (2018).
- [26] G. Concas, J. K. Dewhurst, A. Sanna, S. Sharma, and S. Massidda, Anisotropic exchange interaction between nonmagnetic europium cations in Eu₂O₃, *Phys. Rev. B* **84**, 014427 (2011).
- [27] H. Arizpe-Chávez, F. J. Espinoza-Beltrán, R. Ramirez-Bon, O. Zelaya-Angel, and J. González-Hernandez, Cubic to hexagonal phase transition in CdTe polycrystalline thin films by oxygen incorporation, *Solid State Commun.* **101**, 39 (1997).
- [28] A. Castedo, J. Sanchez, J. Fullea, M. C. Andrade, and P. L. de Andres, *Ab initio* study of the cubic-to-hexagonal phase transition promoted by interstitial hydrogen in iron, *Phys. Rev. B* **84**, 094101 (2011).
- [29] Y. S. You, D. A. Reis, and S. Ghimire, Anisotropic high-harmonic generation in bulk crystals, *Nat. Phys.* **13**, 345 (2017).
- [30] H. Lakhota, M. Zhan, H.-Y. Kim, and E. Goulielmakis, A real space perspective of high harmonic generation in crystalline solids, CLEO, FF2P.5 (2018).
- [31] J. Huster, Die Kristallstruktur von BaTiS₃, *Z. Naturforsch.* **35b**, 775 (1980).
- [32] P. Blaha, K. Schwarz, G. K. H. Madsen, D. Kvasnicka, and J. Luitz, *WIEN2k, An Augmented Plane Wave + Local Orbitals Program for Calculating Crystal Properties* (Karlheinz Schwarz, Techn. Universität Wien, Austria, 2001).
- [33] G. P. Zhang, W. Hübner, G. Lefkidis, Y. Bai, and T. F. George, Paradigm of the time-resolved magneto-optical Kerr effect for femtosecond magnetism, *Nat. Phys.* **5**, 499 (2009).
- [34] G. P. Zhang, Y. H. Bai, and T. F. George, Energy- and crystal momentum-resolved study of laser-induced femtosecond magnetism, *Phys. Rev. B* **80**, 214415 (2009).
- [35] J. P. Perdew, K. Burke, and M. Ernzerhof, Generalized Gradient Approximation Made Simple, *Phys. Rev. Lett.* **77**, 3865 (1996).
- [36] G. P. Zhang and T. F. George, Ellipticity dependence of optical harmonic generation in C₆₀, *Phys. Rev. A* **74**, 023811 (2006).
- [37] T. Hahn, *International Tables for Crystallography* (Kluwer, Dordrecht, 2002).
- [38] M. Lax, *Symmetry Principles in Solid State and Molecular Physics* (Wiley, New York, 1974).
- [39] S. Fagot, P. Foury-Leylekian, S. Ravy, J. P. Pouget, M. Anne, G. Popov, M. V. Lobanov, and M. Greenblatt, Structural aspects of the metal-insulator transition in BaVS₃, *Solid State Sci.* **7**, 718 (2005).